IEEE Photonics Journal
An IEEE Photonics Society Publication

Nanostructured Metal-Enhanced Raman Spectroscopy for DNA Base Detection

Volume 4, Number 5, October 2012

Zhiqian Zhu
Li Zhan
Cailing Hou
Zhimin Wang

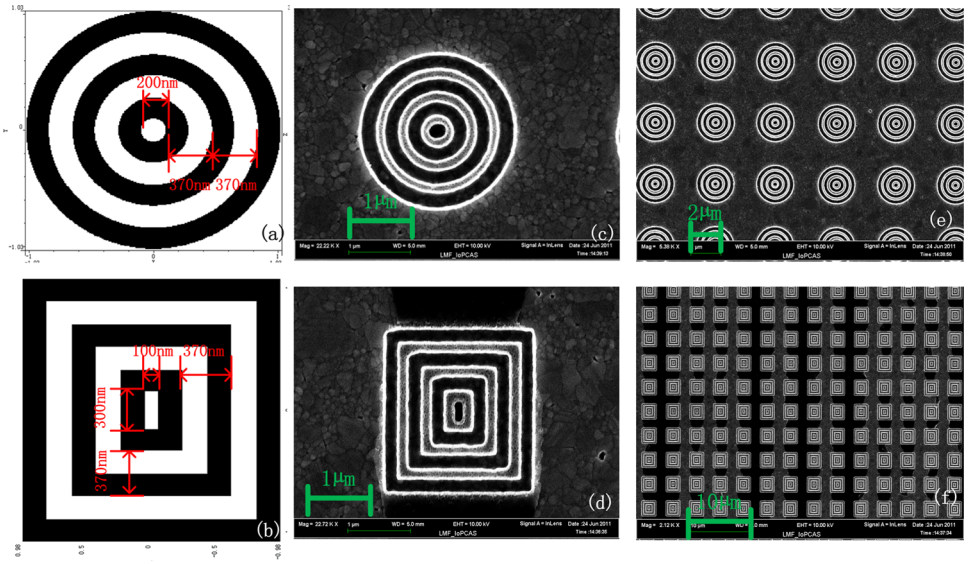

DOI: 10.1109/JPHOT.2012.2208945
1943-0655/$31.00 ©2012 IEEE

IEEE photonics SOCIETY

IEEE

Nanostructured Metal-Enhanced Raman Spectroscopy for DNA Base Detection

Zhiqian Zhu,[1] Li Zhan,[1] Cailing Hou,[2] and Zhimin Wang[2]

[1]Department of Physics, Key Laboratory for Laser Plasmas (Ministry of Education), State Key Lab of Advanced Optical Communication Systems and Networks, Shanghai Jiao Tong University, Shanghai 200240, China
[2]School of Agriculture and Biology, Shanghai Jiao Tong University, Shanghai 200240, China

DOI: 10.1109/JPHOT.2012.2208945
1943-0655/$31.00 ©2012 IEEE

Manuscript received May 9, 2012; revised July 8, 2012; accepted July 10, 2012. Date of publication July 20, 2012; date of current version July 30, 2012. This work was supported by the key project of the Ministry of Education of China under Grant 109061 and by the National Natural Science Foundation of China under Grant 61178014. Corresponding author: L. Zhan (e-mail: lizhan@sjtu.edu.cn).

Abstract: Periodic arrays of subwavelength apertures on Ag film are used as the substrates for nanohole-enhanced Raman spectroscopy. This study presents a rectangular bull's eye structure in an array. We demonstrate the quantitative features of the pattern by the finite-difference time-domain method. This structure is used to enhance the Raman spectroscopy of four DNA bases without labeling. The enhancement factor is up to 10^6. A 1.5-fold enhancement against the circular pattern experimentally confirms the role of sharp corners. This structure may be used in nucleotide identification and DNA sequencing.

Index Terms: Subwavelength structure, sensors, Raman spectroscopy, DNA base detection.

1. Introduction

Raman spectroscopy is a powerful analytical tool because of its nondestructive nature and high-resolution structural fingerprinting details. However, the low sensitivity (typically 10^{-8} quantum yield) of this method is a hindrance to its application. The surface-enhanced Raman scattering (SERS) technique, which has been applied since the 1970s, has made substantial contributions to biological research. An extremely large SERS with a total enhancement factor (EF) on the order of 10^{14} has been obtained at a nonresonant excitation for single molecules attached to Ag clusters [1]. Nevertheless, only the molecular group in direct contact with the metal surface can undergo the enhancement because of the chemical selectivity. The inhomogeneity of clusters also causes difficult reproduction. Recent advances in nanofabrication methods and synthesis have enabled the arrangement of nanoholes into arrays, which can result in unusual physical and chemical properties. Ebbesen *et al.* have reported enhanced light transmission via arrays on Ag film [2]. The metal array appears transparent at a certain wavelength [2], [3]. This development opens a new territory of Raman scattering and sensing. Typical nanohole and nanodisk arrays have been fabricated on metal substrates to enhance Raman signal and instinct fluorescence [4]–[6]. Due to the localized field of surface plasmon resonance (SPR), molecules in subwavelength regions can be detected at low concentrations. The arrays can also serve as SPR sensors because the excitation of surface plasmon polaritons (SPPs) is sensitive to the dielectric constant of cladding [7]–[9]. The miniaturization resulting from the totally small-scale normal incident mode and metal stability offers an approach to the commercial biological sensing chip concept.

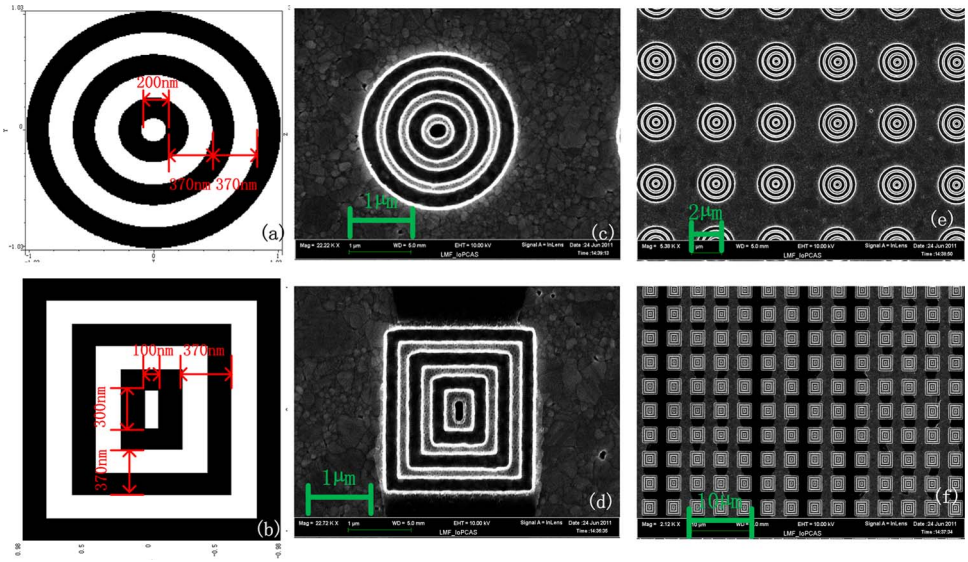

Fig. 1. SEM images and schematic diagram: (a) schematics of the identical circular bull's eye; (b) and identical rectangular pattern; (c) SEM image of the circular pattern; (d) and the rectangular pattern; (e) array of circular bull's eye; (f) array of rectangular pattern. The center aperture and the surrounding corrugations are 80 nm in depth. The film thickness is 200 nm.

In this paper, we report a systematic study of a rectangular-patterned bull's eye array to explore SPR enhancement. The periodic corrugations help to collect the SPPs under normal illumination and concentrate the emission light. Emphasis is given to the localized SP (LSP) near the corner of the metal [10], [11]. We make an attempt to reconstruct the corrugation pattern by introducing sharp corners. This structural design enables the intensive localized fields on a simple bull's eye [12]. The entire active area has a large EF on the order of 10^6 and is within the focal spot $(\sim 1\ \mu m^2)$. The miniaturization of the active area cannot be achieved by a normal nanohole array. The Raman identification of four DNA bases was experimentally demonstrated. Polarization-dependent performance was also observed. In contrast, a 1.5-fold enhancement was achieved on the rectangular pattern. Counter-intuitively, the dipole-like behavior played a negative role here. The results are expected to lay the foundation for nanohole-enhanced Raman scattering without the use of an extrinsic fluorophore. The technology has potential use in DNA identification and sequencing.

2. Theory and Simulation

The structure fabricated by electron beam lithography (EBL) consisted of a 200-nm-thick Ag metal film milled with 100 nm $\times$ 300 nm rectangular apertures surrounded with periodic corrugations. It resembled a so-called bull's eye structure, but we changed the shape from the traditional circle into a rectangle. A circular bull's eye with a 200-nm-diameter center hole was also prepared. Fig. 1 shows a scanning electron microscopy (SEM) image of an identical structure and the array. The total fabrication scale is 0.2×0.2 mm^2 on a 1-cm^2 quartz substrate, on which about 200 periods were fabricated.

A simulated reflection spectrum for normal incident radiation at the center wavelength of 532 nm is shown in Fig. 2(a). The absorption indicated the energy confined to the surface without radiation to induce the localized field. The resonant peaks corresponding to the SP are located at around 550 nm (545 nm for the rectangular pattern and 550 nm for the circular one). The plasmonic resonance spectrally overlaps with the laser light both at excitation and Raman-shifted wavelengths. It benefited the Raman scattering signals. Calculations were performed using the finite-difference time-domain (FDTD) method. The refractive index of Ag was set according to the Drude model [13]. And the potential of the bull's eye as a device element is well recognized: the pattern can give rise to

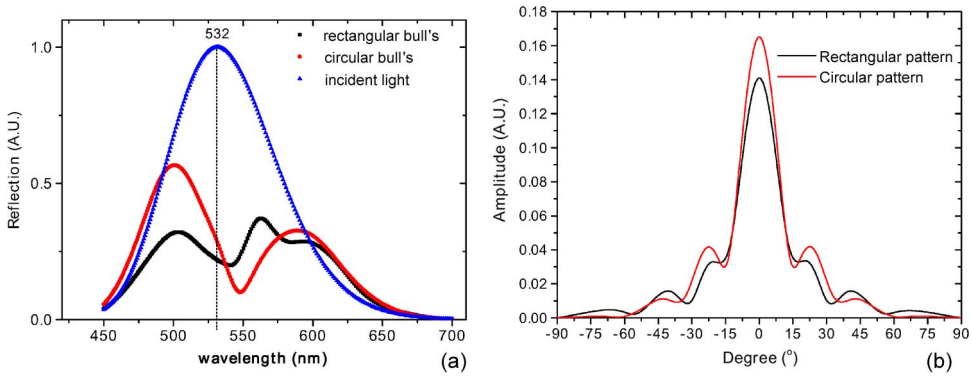

Fig. 2. (a) Calculated incident and reflected spectra of the rectangular pattern (in black) and the circular pattern (in red). (b) Calculated far-field angular distribution of the rectangular pattern along the short axis and circular pattern (in red).

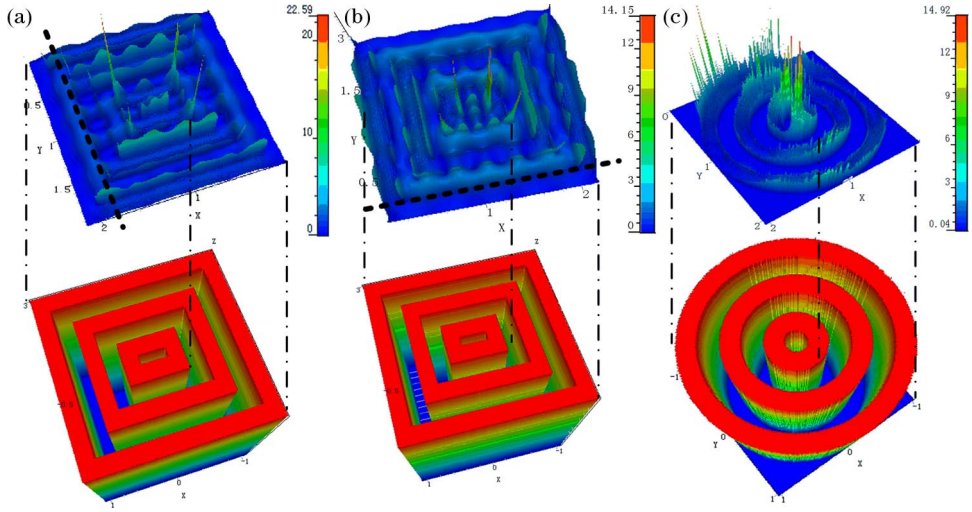

Fig. 3. Calculated near-field intensity image above rectangular pattern (a), (b), and above circular pattern (c). Incident light polarized along the dashed line at a wavelength of 532 nm.

highly directional beaming [14], [15]. Fig. 2(b) presents the far-field distribution (5 mm from the sample) based on the FDTD calculations. Over 84% energy for the rectangular pattern and 90% for the circular pattern were involved in the angle divergence of 60°. The matched condition between the SP momentum and the reciprocal vector of the periodic structure limited the momentum of the reradiated wave. This beaming effect improved the collective efficiency of the microscope [16], [17]. In our experiment, the numerical aperture of the collective lens was 0.5. Accordingly, ~14% of the entire energy flux can be collected into the system. Thus, six times more photons are expected to be detected and eventually converted into electrical signals from the bull's eye.

Besides those properties brought up by bull's eye configuration, some new performances are achieved by the rectangular pattern. The calculated near-field property above the rectangular pattern is presented in Fig. 3(a). The field enhancement reached the maximum at the four corners of the rectangle. Typically, the maximum value of $|E|$ was above 20. This finding implies the EF of $|E|^2$ was 4×10^2. This value was roughly twice the peak value in the circular pattern ($|E|^2 \approx 2.2 \times 10^2$) in Fig. 3(c). The active areas around the corners were anticipated to be optical "hot spots". The DNA molecules located in these areas experienced a much higher excitation field than those

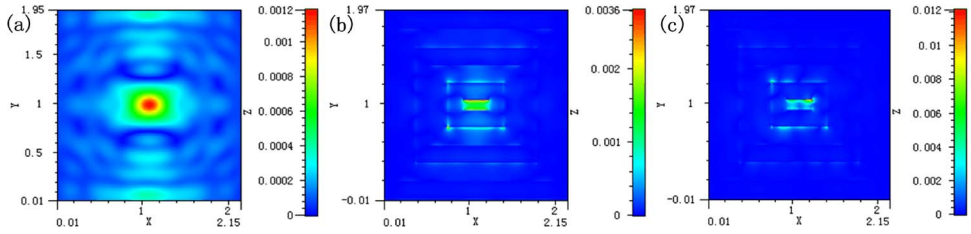

Fig. 4. Calculated near-field intensity above the film of the isolated source point emitting at wavelength of 550 nm (a) without a structure surrounding it, (b) located at the center of the rectangular pattern, (c) located at the top-right corner of the structure.

directly excited by the incident field. Theoretically, the hot spots result from the lightning rod effect [18]. The tips can concentrate more free electrons to induce a largely enhanced field, whereas this highly localized field exhibited an evanescent character that drastically decayed away from the surface [19]. The electric potential can be given as

$$\phi(\rho, \phi) \approx V + a_1 \rho^{\pi/\beta} \sin(\pi\phi/\beta), \tag{1}$$

where β is the angle between the two metal borders, ρ is the distance from the top, and Φ is the azimuth angle inside the given β. In our study, the right angle of the rectangle was $3\pi/2$. Thus, the electric field was proportional to $\rho^{-1/3}$ as a function of distance. This parameter enabled the determination of the evanescent character of the induction field. We assumed the incident field magnitude to be 1; thus, the analytical EF $|E_{loc}/E_{inc}|^2$ was $\sim 4 \times 10^2$. The consistency with the simulation was expected. These accordant results indicated an advantage over the traditional circular pattern, given that more tips were included in the rectangular one. And we can also estimate the tolerance for the roughness of the corners in experimental condition from (1). We can derive the deviation as follows:

$$\Delta E \sim E_{loc} \times \left(\rho^{(\pi/\beta)(\mp\Delta\beta/\beta)} - 1\right). \tag{2}$$

For example, if $\beta = 270^\circ \pm 2^\circ$, we can derive that $\Delta E \sim 10\%$.

Note that $\beta = 3\pi/2$ only indicated that the outside edges of the rectangular side induced the vertex effect. The inner space may play a role as a metal waveguide cavity. As shown in Fig. 3(b), dipolar distribution occurred inside the aperture along with the vertex effect outside. However, the presence of the dipole-like mode reduced the energy concentrated at the corners. It decreased the maximum of the field enhancement.

Radiation from excited-state molecules also plays an important role in the entire Raman scattering procession. Fig. 4 presents the performance of a source point emitting at 550 nm on the rectangular bull's eye structure, which was within the region of the Raman signal in our experiment. Fig. 4(b) indicates that the source point at the center of the structure induced a large excitation field. The dipolar oscillation was observed in the inner space. The excitation source was also dramatically excited to ten times the isolated one when it was located right at the hot spot in Fig. 4(c). This finding corresponded to the lightning rod effect discussed previously.

The EF is related to the electric field both at the excitation and shifted frequencies [6], [13], [20]:

$$G \propto \left|\frac{E_{loc}(\omega_{ex})}{E_0(\omega_{ex})}\right|^2 \times \left|\frac{E_{loc}(\omega_{RS})}{E_0(\omega_{RS})}\right|^2, \tag{3}$$

where $E_{loc}(\omega_{ex})$ is the electric field magnitude at the excitation frequency, $E_{loc}(\omega_{RS})$ is the local electric field of Raman shift frequency, $E_0(\omega_{ex})$ is the incident field at excitation frequency, and $E_0(\omega_{RS})$ is the

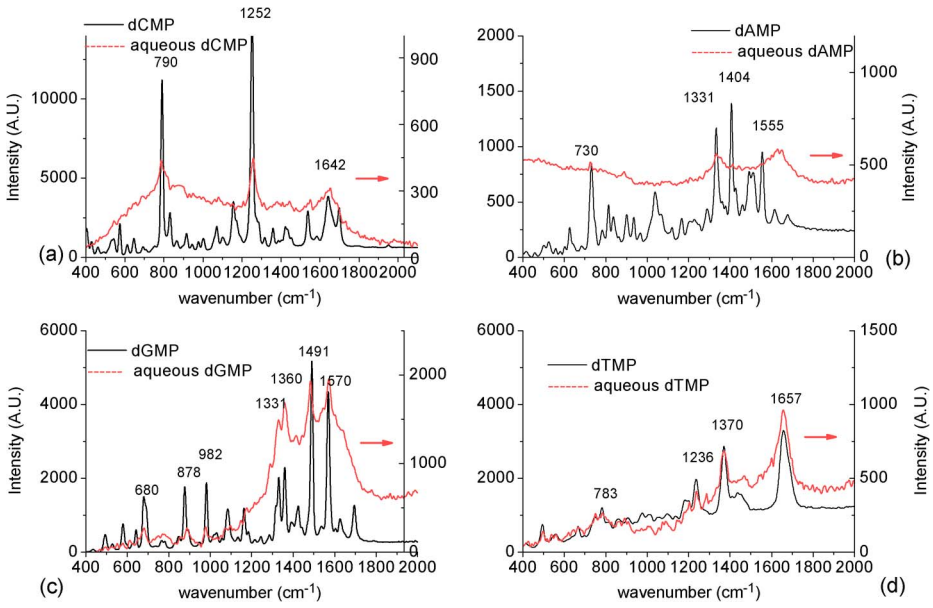

Fig. 5. Raman spectra of 10^{-3} M (a) dCMP, (b) dAMP, (c) dGMP, (d) dTMP in aqueous solution on the rectangular bull's eye (solid red line). The Raman spectra of the four original DNA base powders were also recorded respectively (solid black line).

incident field at the Raman shift frequency. Here, $|E_{loc}(\omega_{ex})/E_{inc}(\omega_{ex})|^2$ was $\sim 4 \times 10^2$ as discussed, and $|E_{loc}(\omega_{RS})/E_{inc}(\omega_{RS})|^2$ was $\sim 10^2$ as shown in Fig. 4(c).

The corrugated configurations benefited the signals with four more tips on each extra groove. More hot spots on the rectangle were involved along with the beaming effect. The contribution at the corners of the outer rectangular-patterned grooves can be found in Fig. 3(a) and (b). By taking the improvement of lens collective efficiency into account, the total EF value can be predicted to be on the order of $10^5 \sim 10^6$ [16], [21], [22].

3. Experimental Results and Discussion

About 10 μL of a 1-mM aqueous solution sample containing decoxyadenosine monophosphate (dAMP), deoxythymidine monophosphate (dTMP), deoxycytidine monophosphate (dCMP), and deoxyguanosine monophosphate (dGMP) was introduced by a micropipette to the substrate for Raman measurements. The samples were placed on a dispersive Raman spectroscope (Bruker Optics). This instrument was equipped with a 50×/0.5 objective lens (focal spot diameter ≈ 1 μm) and a computer-controlled X-Y-Z stage with a 1-μm resolution in the lateral direction. A 532-nm laser with an optional polarizer served as the excitation source at 20 mW ($I \approx 10^5$ W/cm^2). The scattered radiation was collected in the backward direction via the same objective lens and sent to a semiconductor cooled charged-coupled device detector. The signal integration was set to 30 s throughout the experiment.

The enhanced Raman spectra of the four kinds of DNA base molecules absorbed on the rectangular bull's eye array are shown in Fig. 5. The dark lines indicate the ordinary Raman spectra of the pure DNA base sample in powder state for comparison. The enhanced Raman spectra of the 1-mM aqueous base molecule solution are shown by red lines. For the common characteristics of the phosphodiester bond, the peripheral group contributed mainly to the *spectra* from 750 cm^{-1} to 900 cm^{-1}. The major bands between 1300 and 1600 cm^{-1} originated from purine and pyrimidine aromatic rings. The ring breathing mode of dGMP and dAMP can be distinguished at 680 and 730 cm^{-1}, as shown in Fig. 5(b) and (c), respectively [23]. Thus, these eigenvalue peaks corresponding to the breathing mode of carbonyl groups can be used to determine the four kinds of DNA bases readily. The Raman signature of dAMP in water was barely

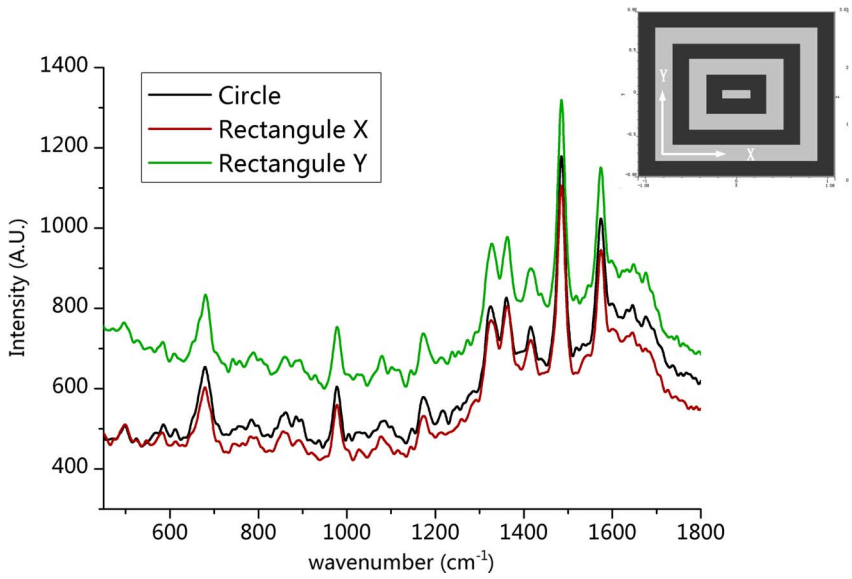

Fig. 6. Raman spectra of dGMP molecule in aqueous solution on circular and rectangular patterns with orthogonal polarizations. The inset illustrates the schematics of the pattern.

recognizable. The intensive noise level resulted from its much lower solubility in water than the other three. Experimental EFs were determined using standard methods [20], [24]. The general equation was

$$G = \frac{I_{surface}/N_{surface}}{I_{bulk}/N_{bulk}}, \tag{4}$$

where I is the intensity of Raman signals, and N is the number of imaged molecules. The substrate was 1×1 cm^2 covered by an aqueous solution, and the diameter of the laser spot was 1 μm. In general, there were about 10^{-17} mol molecules on one single structure. Only half of the molecules residing at the gaps between the neighboring metal corrugations underwent the largest enhancement, and even fewer were located around the corners. Thus, the area-corrected EF was over 3×10^6, consistent with the prediction. For the condition of the experiment, signal from the plate area of the silver film is not detectable above the noise [12].

dGMP exhibited the largest enhancement of Raman scattering followed by dCMP and dTMP in our case. This finding indicated our successive attempt to measure further the performance on the representative dGMP. Fig. 6 gives the polarized performance of the Raman signal of dGMP molecules on the array. The polarization of the electric field was set parallel to the long (X) and short (Y) axes. The polarized incidence on the circular structure was also recorded. For comparison, both arrays were fabricated on the same substrate 5 mm from each other and were only translated with the X-Y stage without changing the focus status during the test. About 1.5-fold enhancement was observed along the two axes. It indicated that the mode polarized perpendicular to the long axis was more enhanced than that to the short axis. This result implied that the X-polarized incident more easily induced the dipole-like mode on the pattern, sharing the energy from four corners as aforementioned. The noise-to-signal ratio improved in the polarization pattern compared with the normal spectrum in Fig. 5(c). This phenomenon aided the achievement of a high-resolution Raman spectrum in aqueous solution.

4. Conclusion

Nanostructured metal-enhanced Raman scattering is demonstrated on a rectangular bull's eye array structure on Ag film. This pattern benefits the excitation of SPs and intensive localized field in

one simple structure. The localized fields from the sharp corners play crucial roles in contributing to the EF on the order of 10^6. The Raman spectra of four DNA base molecules are obtained without extrinsic labeling. These findings may provide an attractive way for sensing elements on transport flow by equipped microfluidic configuration and also for single-molecule on-chip detection with a very small-scale volume.

Acknowledgment

The authors would like to thank Z. Y. Fan in Ohio University for useful discussions.

References

[1] K. Kneipp, Y. Wang, H. Kneipp, L. T. Perelman, I. Itzkan, R. R. Dasari, and M. S. Feld, "Single molecule detection using surface-enhanced Raman scattering (SERS)," *Phys. Rev. Lett.*, vol. 78, no. 9, pp. 1667–1670, Mar. 1997.
[2] T. W. Ebbesen, H. Lezec, H. Ghaemi, T. Thio, and P. Wolff, "Extraordinary optical transmission through sub-wavelength hole arrays," *Nature*, vol. 391, no. 6668, pp. 667–669, Feb. 1998.
[3] C. Genet and T. Ebbesen, "Light in tiny holes," *Nature*, vol. 445, no. 7123, pp. 39–46, Jan. 2007.
[4] A. G. Brolo, E. Arctander, R. Gordon, B. Leathem, and K. L. Kavanagh, "Nanohole-enhanced Raman scattering," *Nano Lett.*, vol. 4, no. 2, pp. 2015–2018, Oct. 2004.
[5] J. T. Bahns, Q. Guo, J. M. Montgomery, S. K. Gray, H. M. Jaeger, and L. Chen, "High-fidelity nano-hole-enhanced Raman spectroscopy," *J. Phys. Chem. C*, vol. 113, no. 26, pp. 11 190–11 197, Jul. 2009.
[6] M. H. Chowdhury, K. Ray, M. L. Johnson, S. K. Gray, J. Pond, and J. R. Lakowicz, "On the feasibility of using the intrinsic fluorescence of nucleotides for DNA sequencing," *J. Phys. Chem. C*, vol. 114, no. 16, pp. 7448–7461, Apr. 2010.
[7] A. G. Brolo, R. Gordon, B. Leathem, and K. L. Kavanagh, "Surface plasmon sensor based on the enhanced light transmission through arrays of nanoholes in gold films," *Langmuir*, vol. 20, no. 12, pp. 4813–4815, Jun. 2004.
[8] K. A. Tetz, L. Pang, and Y. Fainman, "High-resolution surface plasmon resonance sensor based on linewidth-optimized nanohole array transmittance," *Opt. Lett.*, vol. 31, no. 10, pp. 1528–1530, May 2006.
[9] A. A. Yanik, A. E. Cetin, M. Huang, A. Artar, S. H. Mousavi, A. Khanikaev, J. H. Connor, G. Shvets, and H. Altug, "Seeing protein monolayers with naked eye through plasmonic Fano resonances," in *Proc. Nat. Acad. Sci.*, 2011, Jul. 2011, vol. 108, no. 29, pp. 11 784–11 789.
[10] K. Ueno, S. Takabatake, Y. Nishijima, V. Mizeikis, Y. Yokota, and H. Misawa, "Nanogap-assisted surface plasmon nanolithography," *J. Phys. Chem. Lett.*, vol. 1, no. 3, pp. 657–662, Feb. 2010.
[11] K. J. K. Koerkamp, S. Enoch, F. Segerink, N. Van Hulst, and L. Kuipers, "Strong influence of hole shape on extraordinary transmission through periodic arrays of subwavelength holes," *Phys. Rev. Lett.*, vol. 92, no. 18, pp. 183901-1–183901-4, May 2004.
[12] Q. Min, M. J. L. Santos, E. M. Girotto, A. G. Brolo, and R. Gordon, "Localized Raman enhancement from a double-hole nanostructure in a metal film," *J. Phys. Chem. C*, vol. 112, no. 39, pp. 15 098–15 101, Oct. 2, 2008.
[13] D. Lin, Y. Chen, P. Jhuang, J. Chu, J. Yeh, and J. K. Wang, "Optimizing electromagnetic enhancement of flexible nano-imprinted hexagonally patterned surface—Enhanced Raman scattering substrates," *Opt. Exp.*, vol. 19, no. 5, pp. 4337–4345, Feb. 2011.
[14] H. Caglayan, I. Bulu, and E. Ozbay, "Beaming of electromagnetic waves emitted through a subwavelength annular aperture," *J. Opt..Soc. Amer. B*, vol. 23, no. 3, pp. 419–422, Mar. 2006.
[15] O. Mahboub, S. C. Palacios, C. Genet, F. Garcia-Vidal, S. G. Rodrigo, L. Martin-Moreno, and T. Ebbesen, "Optimization of bull's eye structures for transmission enhancement," *Opt. Exp.*, vol. 18, no. 11, pp. 11 292–11 299, May 2010.
[16] A. Ahmed and R. Gordon, "Directivity enhanced Raman spectroscopy using nanoantennas," *Nano Lett.*, vol. 11, no. 4, pp. 1800–1803, Apr. 13, 2011.
[17] A. Ahmed and R. Gordon, "Single molecule directivity enhanced Raman scattering using nanoantennas," *Nano Lett.*, vol. 12, no. 5, pp. 2625–2630, May 9, 2012.
[18] L. Novotny and B. Hecht, *Principles of Nano-Optics*. Cambridge, U.K.: Cambridge Univ. Press, 2006, p. 193.
[19] J. Jackson and R. K. P. Zia, *Classical Electrodynamics,* 2nd ed. New York: Wiley, 1975, p. 85.
[20] T. H. Reilly, III, S. H. Chang, J. D. Corbman, G. C. Schatz, and K. L. Rowlen, "Quantitative evaluation of plasmon enhanced Raman scattering from nanoaperture arrays," *J. Phys. Chem. C*, vol. 111, no. 4, pp. 1689–1694, Feb. 2007.
[21] S. Zou and G. C. Schatz, "Silver nanoparticle array structures that produce giant enhancements in electromagnetic fields," *Chem. Phys. Lett.*, vol. 403, no. 1–3, pp. 62–67, Feb. 2005.
[22] R. Adato, A. A. Yanik, J. J. Amsden, D. L. Kaplan, F. G. Omenetto, M. K. Hong, S. Erramilli, and H. Altug, "Ultra-sensitive vibrational spectroscopy of protein monolayers with plasmonic nanoantenna arrays," *Proc. Nat. Acad. Sci.*, vol. 106, no. 46, pp. 19 227–19 232, Nov. 2009.
[23] G. D. Chumanov and T. M. Cotton, "Surface-enhanced Raman scattering for discovering and scoring single-base differences in DNA," *Proc. SPIE*, vol. 3608, no. 1, pp. 204–210, Apr. 1999.
[24] R. Van Duyne, J. Hulteen, and D. Treichel, "Atomic force microscopy and surface-enhanced Raman spectroscopy. I. Ag island films and Ag film over polymer nanosphere surfaces supported on glass," *J. Chem. Phys.*, vol. 99, no. 3, pp. 2101–2115, 1993.